ELSEVIER

Journal of Nuclear Materials 253 (1998) 87–103

journal of nuclear materials

Section 3. Fundamental radiation effects

Topological modeling of amorphized tetrahedral ceramic network structures

C. Esther Jesurum [b,c], Vinay Pulim [c], Linn W. Hobbs [a,*]

[a] *Department of Materials Science and Engineering, Room 13-4062, MIT, 77 Massachusetts Avenue, Cambridge, MA 02139-4307, USA*
[b] *Department of Mathematics, Massachusetts Institute of Technology, Cambridge, MA 02139, USA*
[c] *Laboratory for Computer Science, Massachusetts Institute of Technology, Cambridge, MA 02139, USA*

Abstract

The topology of the tetrahedral network compounds SiO_2, Si_3N_4 and SiC is considered and applied to the potential for amorphization of these compounds. Local rules are devised for self-assembly modeling of crystalline polymorphs of the latter two, similar to those derived previously for SiO_2, and modifications of these rules are applied to generate topologically disordered versions. Success in obtaining viable amorphous networks is assessed in terms of residual underconnection, tetrahedral distortion, partial radial correlations, and local clusters of tetrahedra that embody the local topology. Topologically assembled models of amorphous Si_3N_4 are found to be constructible, but with radial correlations and local clusters much closer to those of the parent crystals than for assembled amorphous models of silica. Models of amorphous SiC remain substantially underconnected and highly distorted tetrahedrally; the seemingly contrary experimentally observed facile amorphization of SiC under irradiation is suggested to be facilitated by the potential for chemical disorder in SiC that alters the topological possibilities. © 1998 Elsevier Science B.V.

1. Introduction

Network structures are atomic arrangements that are principally characterized by skeletal connectivity of discrete structural units. Polymers [1] are one class of network structures, as are most biological molecular assemblages such as virus shells comprised of assembled proteins [2]. SiO_2, Si_3N_4 and SiC are three ceramic compounds that adopt network structures featuring vertex sharing of, respectively, $[SiO_4]$, $[SiN_4]$ and $[SiC_4]$ tetrahedra. Silicas, which are found in both crystalline and aperiodic structures, are critical elements in frequency control (piezoelectric crystalline quartz) and optical telecommunication (vitreous silica fibers). Silicon nitride, found in α and β crystalline polymorphs, is an important structural ceramic and fiber-reinforced composite matrix, while silicon carbide, also found in two polymorphic forms α and β and numerous polytypic variants, is a principal reinforcing fiber, a potential high-temperature device semiconductor, and a leading candidate (in SiC–SiC fiber-reinforced ceramic matrix composite form) for near-first-wall applications in thermonuclear fusion reactors.

The connectivity of $[SiX_4]$ tetrahedra (X = O, N or C) in networks of the three compounds is illustrated in Fig. 1. In silicas, each of the four vertices of an $[SiX_4]$ tetrahedron (X = O) is shared by two tetrahedra ({4,2} connectivity); in silicon nitride (X = N) by three tetrahedra ({4,3} connectivity); and in silicon carbide (X = C) by four tetrahedra ({4,4} connectivity). These respective connectivities obtain for all known crystalline polymorphs of the three compounds except the high-pressure stishovite form of SiO_2. Crystals exhibit *topological order*, that is, translational periodicity and rotational invariance [3]. The evidence from Raman spectroscopy, X-ray absorption and electron inelastic scattering fine structures, and X-ray, neutron and electron diffraction studies is that {4,2} connectivity also obtains in vitreous silica as well, which is topologically *dis*ordered.

Networks are not constrained to be *crystalline* arrangements of connected polyhedra; highly covalent networks, especially, are more likely to be found in non-crystalline

* Corresponding author. Tel.: +1-617 253 6835; fax: +1-617 252 1020; e-mail: hobbs@mit.edu.

PII S0022-3115(97)00363-2

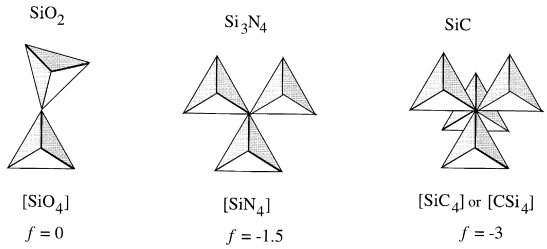

Fig. 1. Vertex-sharing schemes for SiO_2, Si_3N_4 and SiC.

forms than are less covalent, more highly connected ceramics such as ionic oxides [4]. Silica, for example, is easily amorphized by cooling moderately quickly from its liquid (forming vitreous silica), by gas-phase deposition, by high-temperature oxidation of Si, or by radiation involving both radiolytic and ballistic atomic displacements [5]. Si_3N_4, on the other hand, appears difficult to amorphize by radiation [6] and has been rendered aperiodic mostly in molecular dynamics (MD) simulations [7,8]. The relative amorphizabilities of SiO_2 (two tetrahedra sharing a vertex) and Si_3N_4 (three tetrahedra sharing a vertex) in fact correlate well with the structural freedom f (defined as the degrees of freedom per tetrahedron vertex less the number of constraints imposed by the connectivity [9–11]) available to their respective structures to rearrange, as discussed in Section 2.

In an earlier paper [12], we have shown that {4,2} crystalline silica networks can be assembled using a compact set of *local assembly rules* that do not rely on long-range symmetry operations and are thus applicable to the construction of topologically disordered as well as topologically ordered network structures. Local rules for assembly of topologically disordered structures can be derived from modifications of the crystalline assembly rules. The local structure of assembled silica networks—crystalline or amorphous—can then be described adequately by a partial tessellation called the *local cluster* which fully embeds the local topology. In this contribution, we first describe local rules-based assembly of crystalline SiO_2, SiC and Si_3N_4 polymorphs, then explore the comparative feasibility of erecting topologically disordered versions using altered rules. In a companion paper [13], we investigate amorphization of these three compounds by disordering and reassembly algorithms that simulate collision cascades during ion irradiation. We conclude with an assessment of the observed role of topological constraints on amorphization of these network ceramics.

2. Structural freedom of Si–X networks

For purely vertex-sharing polyhedral networks, the degree of structural freedom f at each vertex (equal to the number of degrees of freedom d less the number of constraints h imposed by neighboring structure) has been deduced by Gupta and Cooper [4] to be

$$f = d - h = d - C\left[\delta\{\delta - (\delta + 1)/2V\}\right], \qquad (1)$$

where $d = 3$ for three-dimensional assemblies, δ is the dimensionality of the structuring polytope (3 for a tetrahedron), and the structural connectivity, represented as $\{V,C\}$, derives from the number of vertices V per polytope (4 for a tetrahedron) and the number of polytopes C per vertex. Values of f for the three Si–X compounds and for elemental Si are given in Table 1, together with amorphization fluences (expressed as deposited energy density in eV/atom) for heavy ion irradiation well below the threshold temperature for amorphization. For {4,2}-connected SiO_2, $f = 0$, and all tetrahedral silica polymorphs amorphize easily (~ 7 eV/atom for quartz [16]). By contrast, the more-connected {4,3} silicon nitride has $f = -1.5$ and is very difficult to amorphize without accompanying chemical effects of the implanted ion. [1]

The added connectivity of SiC networks (four tetrahedra sharing a vertex) confers still less structural freedom and the least expected amorphizability of the three compounds. But SiC is, connectivity notwithstanding, easily amorphized by ballistic displacement involving electron irradiation (critical displacement energy deposition density ~ 90 eV/atom) [18–21] or ion irradiation (~ 16 eV/atom for α-SiC, ~ 21 eV/atom for β-SiC) [14,22–26] well below a surprisingly high threshold amorphization temperature (~ 295 K for electrons and ~ 485 K (α) or ~ 498 K (β) for ions, depending to some extent on ion mass and energy [23,24,26]). We have made the suggestion previously [11] that topological disorder in SiC is likely only if anti-site disorder (C on Si sites and vice-versa, generating $[CC_4]$ and $[SiSi_4]$ tetrahedra) is present or induced, and indeed there is now recent Raman and EXAFS experimental evidence [25] to suggest that radiation-amorphized SiC has been modified in this way. The Si–C, Si–Si and C–C covalent bond energies are respectively 317, 221 and 347 kJ/mol [27], which implies that the bond energies associated with a $[CC_4]$ tetrahedron (1388 kJ/mol) resulting from chemical disorder is actually greater than that for a $[SiC_4]$ tetrahedron (1268 kJ/mol), while the average of the $[CC_4]$ and $[SiSi_4]$ anti-site pair of tetrahedra (1136

[1] Irradiating at 300 K, in the absence of any such contribution, Si_3N_4 could not be amorphized after 700 eV/atom [6], but an amorphization threshold temperature for Si_3N_4 has not been established. A temperature dependence for amorphization between 80 K and 420 K has been noted [17], although the irradiations used almost certainly involved a chemical contribution from the implanted ion. While it is thus conceivable that 700 eV/atom may not represent a *lowest* bound critical amorphization dose for irradiation at lower temperatures, Si_3N_4 is nonetheless vastly less amorphizable than SiO_2.

Table 1
Coordination, connectivity, structural freedom and amorphizability for Si–X structures

Structure	Polyhedra: sharing	{*V*, *C*}	*f*	Amorphization dose (eV/atom)[a]
SiC	Tetrahedra: corners	{4,4}	−3	16 [14]
Si_3N_4	Tetrahedra: corners	{4,3}	−1.5	> 700[b] [6]
SiC	*Tetrahedra: corners*	*{4,2}*	< 0	16 [14]
Si	*Tetrahedra: corners*	*{4,2}*	0	11 [15]
SiO_2	Tetrahedra: corners	{4,2}	~ *0*	7 [16]
Si	Rods: ends	{2,4}	< +1	11 [15]

[a] Low-temperature values of critical energy density required for amorphization.
[b] Room-temperature value.
Italicized entries are based on atom-centered polytopes which are not coordination polyhedra (see text).

kJ/mol) is not much less than for the $[SiC_4]$ tetrahedra that comprise the structure; these bond energetics are possibly related to why SiC dissociates before it melts. The production (e.g., by replacement collisions) of $[CC_4]$ tetrahedra, which represent the lowest energy C_{Si} anti-site defect, and whose existence in irradiated SiC the Raman and EXAFS measurements apparently confirm, creates local sub-units of cubic diamond; Si_C anti-site defects similarly create sub-units of Si.

While definitive low-temperature amorphization experiments have not been carried out for diamond carbon, measurements have been made for elemental crystalline Si [15], which shares the diamond–cubic structure. Topologically, crystalline Si can be viewed as a {2,4} network of Si–Si bond rod polytopes, yielding $f = +1$, but this representation underrepresents the rigidity of the Si tetrahedral sp^3 hybridized bond angle. A better polytopic representation is a set of {4,2}-connected tetrahedra with vertices at the bond midpoints and a Si–midpoint–Si angle $\theta = 180°$, as in ideal cristobalite that can be derived from Si by decorating the bond midpoints with oxygen. It should be noted that this representation still slightly overestimates the structural freedom at $f = 0$, because the Si–Si bonds are constrained to be linear (except in bridging around Si vacancies [28]), whereas θ for silicas is easily varied between 130° and 180° [12,29]. The observed amorphizability of Si (11 eV/atom for ion irradiation [15]) is consistent with this topological representation. The observed amorphizability of SiC (as low as 16 eV/atom for ion irradiation) – not much more difficult than Si and considerably easier than implied by its {4,4} connectivity – is accordingly consistent with partial chemical disorder, induced by the displacive radiation, conferring a more Si-like local topology.

The single displacements characteristic of electron irradiation exhibit a replacement/displacement ratio at least an order of magnitude lower than for cascade displacements [23,26]. The dependence of SiC amorphization on prior induced chemical disorder could thus certainly explain the higher critical displacement energy density for electron irradiation compared to ion irradiation, as well as the observed dependence of amorphization dose on PKA energy [24]. It may also explain the lower amorphization threshold temperature for electron irradiation: higher dynamic annealing temperatures are needed to recover the higher chemical disorder that accumulates from ion irradiation.

3. Local rules-based structure assembly

Atoms in a structure do not possess global information, such as that embodied in symmetry operations, but instead respond to local forces in their immediate environment as they assemble into a structural arrangement. The same is true of larger assembly units, such as proteins whose self-assembly into icosahedral virus shells can be replicated using only a combinatorial set of local rules based on pairwise interactions between adjacent proteins [2]. We have shown [12] that a similar rules-based approach, using tetrahedra as building blocks, permits rapid self-assembly of {4,2} tetrahedral networks of silica in all their polymorphic variety. The approach is equally applicable to the more connected {4,3} tetrahedral networks of Si_3N_4 and {4,4} tetrahedral networks of SiC. The modeling of amorphous silicon carbide (a–SiC) described in Section 4 explores the consequences of attempting to impose topological disorder on this compound in the absence of chemical disorder.

3.1. Local rules for self-assembly of tetrahedral crystalline polymorphs

The local rules for assembly of vertex-sharing tetrahedra require a knowledge of the number of topologically inequivalent environments about the tetrahedra (number of types), the number of additional tetrahedra sharing a given vertex (their connectivity), the orientation of the starting tetrahedron (initial node orientation), and instructions regarding the relative orientation and type of each neighboring tetrahedron to which each vertex of the starting tetrahedron connects (vertex rules). We arbitrarily specify a

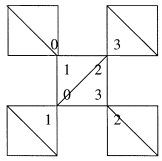


```
Beta-Cristobalite
1
4 1
REGULAR
y 23 ;
0 1  z 90 ;
0 0  z -90 ;
0 3  z 90 ;
0 2  z -90 ;
```

```
a-Cristobalite
1
4 1
REGULAR
y 23 ;
0 1  z 85 ;
0 0  z -85 ;
0 3  z 85 ;
0 2  z -85 ;
```

Fig. 2. Assembly rules for two SiO_2 polymorphs. (a) (top) crystalline β-cristobalite, (b) (bottom) an amorphous-SiO_2 based on modification of β-cristobalite rules. The rules for α-cristobalite are identical to those for β-cristobalite but with an initial offset of 24.7° instead of 23° about *y*.

canonical orientation for the starting tetrahedron by inscribing it in a unit cube centered at the origin, with vertices labelled 0,1,2,3 at four cube corners. A rotation is applied to this canonical tetrahedron to define the orientation of the initial node, as defined by rotations about the *x*, *y* and *z* axes of the unit cube. The rules for each vertex will dictate the position of one (SiO_2), two (Si_3N_4), or three (SiC) neighboring tetrahedra.

Fig. 2a illustrates a rules set for assembling crystalline β-cristobalite; rules for quartz and other silica polymorphs are described in our previous treatment of silica [12]. The first line in the rules file enumerates the number of node types (in this case only one, because all tetrahedra share identical environments). The second line indicates the network connectivity; '4 1' signifies a structure in which each polyhedral subunit has four vertices (a tetrahedron) and each vertex seeks one neighbor (so that two tetrahedra share a vertex). The third line indicates that the tetrahedron is regular; if it is not, we must additionally specify the initial coordinates of its vertices (we have assumed the tetrahedra to be regular, with intra-tetrahedral X–Si–X angle of 109.5°, recognizing that small tetrahedral distortions exist in some crystalline polymorphs). The fourth line specifies any rotation applied to the initial canonical node orientation, resolved into rotations about *x*, *y* and *z* (in this case, a 23° rotation about *y*). This node offset turns ideal cristobalite, with an Si–O–Si inter-tetrahedral angle $\theta = 180°$, into β-cristobalite with $\theta = 148°$. The remaining four lines summarize the assembly rules at each vertex. The first of these specifies the rule for vertex 0 (in this case, vertex 0 is connected to a tetrahedron of type 0 at its vertex 1, rotated 90° about the *z* axis). The next three lines give the node type, vertex numbers and rotations of neighboring tetrahedra connected to the remaining vertices of the initial node.

These rules are then applied to each of the added tetrahedra in turn, and so on until a structure of desired size is assembled. Assembly and subsequent analyses of bond angles, density, topology and radial correlations were all carried out on a Silicon Graphics Onyx workstation, using an efficient graphical user interface that was developed specifically for the purpose. Tetrahedra were assembled at a rate of about 5 Hz (limited by the graphic display rate), and networks of 1500–10 000 tetrahedra were typically assembled for analysis, large enough to minimize surface effects. Illustrations of the crystalline assemblies in this publication are restricted to 1000 tetrahedra for clarity. Fig. 3a shows 200 tetrahedra assembled according to the rules for β-cristobalite specified in the Fig. 2a rules file. The simulations record all vertex coordinates and the complete adjacency matrix, so that calculation of density, intra- and inter-tetrahedral angles, and radial correlations can be made at each tetrahedron site.

Fig. 4 compares 200-tetrahedron assemblies of β- and α-Si_3N_4, following the assembly sequences and local rules given in Figs. 5 and 6. Fig. 5a depicts the assembly sequence and provides the assembly rules file for β-Si_3N_4, which is the simpler of the two silicon nitride crystalline polymorphs. Three tetrahedra, all of the same node type (type 0) share a N vertex in silicon nitride, so each vertex seeks two additional tetrahedra, whose rotation rules appear in two separate sets. In α-Si_3N_4, there are two distinguishable tetrahedral environments, but four tetrahedron node types (0, 1, 2 and 3) were, in practice, used to render the modeling conceptually simpler. The rules for each of the four types are given in Fig. 6, together with a depiction of the assembly scheme. These four tetrahedron node types are separately distinguished in Fig. 4b. Examination of the Si–N–Si angle θ for the four α-Si_3N_4 tetrahedron node types in Table 2 (two of which should be equivalent) reveals that our rules for α-Si_3N_4 are not quite perfect, but are considered close enough for modeling purposes.

Figs. 7 and 8a depict the assembly sequences and rules files for β- (3C) and α- (6H) SiC polytypes. In both {4,4}-connected structures, four [SiC_4] (or [CSi_4]) tetrahedra share a vertex, so each vertex seeks connections with three other tetrahedra, all of the same type. Two of these connections are made in a plane of linked tetrahedra with identical orientations (a {111} plane in β-SiC, the (0001) basal plane of α-SiC); in β-SiC, the third connection is made with a tetrahedron belonging to an identical plane above, in α-SiC with one belonging to a similar plane rotated 180° about the [0001] axis. Fig. 9 compares assemblies of 200 tetrahedra of each structure.

Model densities were calculated from the reported Si–X distance and the number of tetrahedra in a selected volume of the model; the latter was determined by centering a sphere slightly smaller than the convex hull (largest polyhedron with triangular faces containing all nodes) randomly in turn on 10 interior nodes and counting and

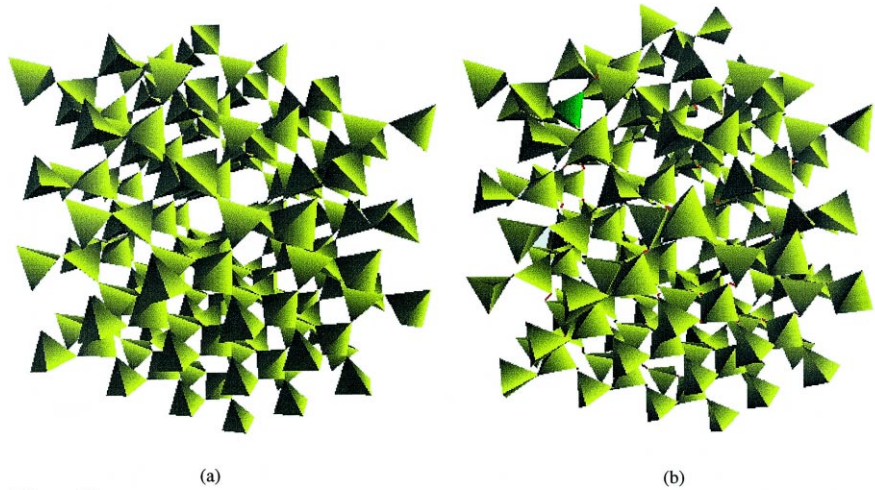

Fig. 3

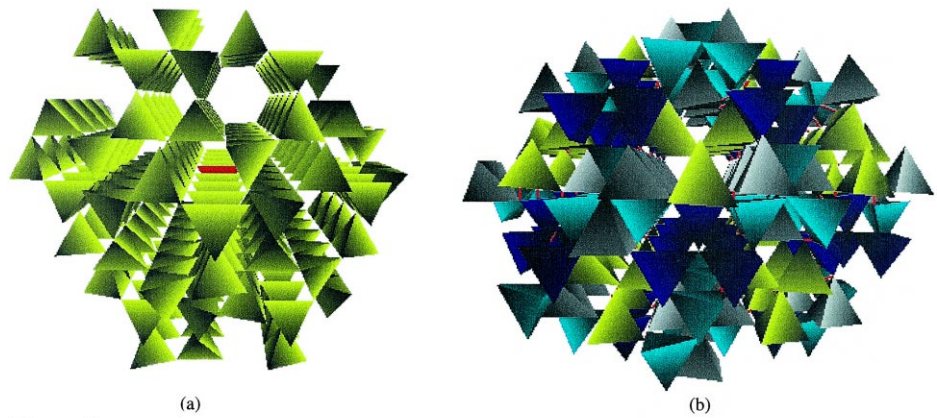

Fig. 4

Fig. 3. 200-tetrahedra models of SiO_2 assembled according to the rules for (a) β-cristobalite given in Fig. 2a, and (b) cristobalite-like a-SiO_2 given in Fig. 2b. Green tetrahedra in (b) are underconnected, and red segments are remanent connection springs.

Fig. 4. 200-tetrahedron models of (a) β-Si_3N_4, assembled according to the rules following in Fig. 5a, and (b) α-Si_3N_4, assembled according to the rules following in Fig. 6.

averaging the number of tetrahedra in each case enclosed by the spheres. Si–X distances used were, for Si–O, 0.162 nm; for Si–N, 0.173 nm; and for SiC, 0.188 nm. Computed densities, together with corresponding inter- and intra-tetrahedral angles, are given in Table 2, where they are compared to experimental values. For example, the computed density for the β-cristobalite model in Fig. 3a was 2.17 ($\times 10^3$ kg/m^3) compared to the experimental value of 2.21; values for Si_3N_4 and SiC were even closer. Densities were found to depend sensitively on the initial node orientation [12], which for cristobalite was chosen to yield the experimental Si–O–Si bond angle and for Si_3N_4 and SiC to correctly reproduce the crystal structures. Partial radial density correlation functions for Si–X, X–X and Si–Si were computed from the vertex coordinates, using counting algorithms described earlier [12], for comparison to those from topologically disordered models described in Section 4. Topological properties of the models were deduced from the adjacency matrix, as outlined in Section 3.2.

3.2. Topological representation of assembled networks

A real network of fully connected vertex-sharing tetrahedra may be represented mathematically as a regular graph in which the tetrahedra comprise network nodes and connections between nodes exist where the corresponding tetrahedra share corners. The real network of tetrahedra

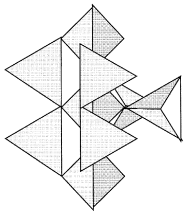

```
Beta-Si3N4
1
4 2
REGULAR
z 45 ;
0 1  y  60 ;   0 2  ;
0 0  y -60 ;   0 2  y  -60 ;
0 1  y  60 ;   0 0  ;
0 3  y 120 ;   0 3  y -120 ;
```

```
a-Si3N4
1
4 2
REGULAR
x 5 z 45 ;
0 1  y  55 ;   0 2  ;
0 0  y -55 ;   0 2  y  -65 ;
0 1  y  65 ;   0 0  ;
0 3  y 120 ;   0 3  y -120 ;
```

Fig. 5. Assembly sequence and assembly rules for (a) (top) β-Si_3N_4, and (b) (bottom) an a-Si_3N_4 based on modification of the β-Si_3N_4 rules.

and its nodal graph representation possess isomorphic topologies [5,12], which are fully describable only by a complete tessellation, for example, by the set of three-dimensional void polyhedra bounded by the node connections [32]. A simpler *partial* tessellation, based on *rings* (a topologically one-dimensional entity), has been shown [5] to describe the structural topology—adequately enough to differentiate all tetrahedral polymorphs of silica [12].

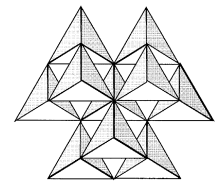

```
Beta-SiC
1
4 3
REGULAR
;
0 1  ;   0 2  ;   0 3  ;
0 0  ;   0 2  ;   0 3  ;
0 0  ;   0 1  ;   0 3  ;
0 0  ;   0 1  ;   0 2  ;
```

Fig. 7. Assembly sequence and assembly rules for β-SiC.

A ring is a closed circuit along nodal connections, and rings must exist in networks if the inevitable density catastrophe of tree networks is to be avoided. The circuits that are topologically important, known as *primitive* rings [33] but hereafter sometimes referred to simply as *rings*, are those minimal circuits that are not the sum of two smaller circuits. The primitive ring-finding algorithm used in this study, details of which are given elsewhere [12], involves enumeration of the *closest* nodes in turn to find all simple paths originating and terminating at a network node *n*, where a simple path has no node appearing more than once. For each pair of nodes on the path, the graph distance between them is then ascertained to be equal to the minimum ring distance between the two nodes. We enumerate all rings associated with *each node*, testing for primitiveness in turn, which is more efficient for small samples than first computing all rings in the *network* [34]

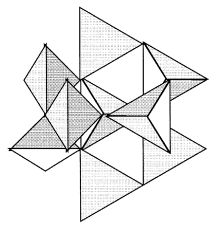

```
Alpha-Si3N4
4
4 2
REGULAR
x -45 y 29 ;
1 0  ;         2 2  y  -60 ;
1 1  ;         3 2  y   60 ;
2 0  y  60 ;   3 0  y  -60 ;
0 3  y 120 ;   0 3  y -120 ;
```

```
4 2
REGULAR
x -45 y 29 x 180 ;
0 0  ;         2 2  y  -60 ;
0 1  ;         3 2  y   60 ;
2 1  y  60 ;   3 1  y  -60 ;
1 3  y 120 ;   1 3  y -120 ;
```

```
4 2
REGULAR
x -45 y 29 x 180 ;
3 0 y -120 ;   0 2  y  -60 ;
1 1 y -120 ;   1 2  y  -60 ;
0 0  y  60 ;   1 0  y   60 ;
2 3  y 120 ;   2 3  y -120 ;
```

```
4 2
REGULAR
x -45 y 29 ;
2 0  y 120 ;   0 2  y   60 ;
2 1  y 120 ;   1 2  y   60 ;
0 1  y  60 ;   1 1  y  -60 ;
3 3  y 120 ;   3 3  y -120 ;
```

Fig. 6. Assembly sequence and assembly rules for α-Si_3N_4.

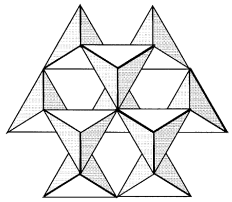

```
Alpha-SiC
1
4 3
REGULAR
x -45 y -144.8 z 90 ;
0 1       ;  0 2       ;  0 3  z 180 ;
0 0       ;  0 2       ;  0 3  z 180 ;
0 0       ;  0 1       ;  0 3  z 180 ;
0 0 z 180 ;  0 1 z 180 ;  0 2  z 180 ;
```

```
a-SiC
1
4 3
REGULAR
x -40 y -144.8 z 90 ;
0 1   x 5 ;  0 2   x 5 ;  0 3  z 175 ;
0 0  x -5 ;  0 2   x 5 ;  0 3  z 175 ;
0 0  x -5 ;  0 1  x -5 ;  0 3  z 175 ;
0 0 z -175;  0 1 z -175;  0 2  z -175;
```

Fig. 8. Assembly sequence and assembly rules for (a) (top) α-SiC and (b) (bottom) an a-SiC based on modification of α-SiC rules.

and then testing for primitiveness. Additionally, the searches at each node were truncated at rings of maximum length < 20, which proved adequate.

The set of nodes (tetrahedra) belonging to all primitive rings which pass through a given node *n* is defined as the *local cluster* of that node. The local cluster specifies the local environment and distinguishes the local topologies in much the same way that the unit cell of a crystal specifies the local environment and identifies the crystal symmetries; the local cluster has the added advantage of applying to non-crystalline structures as well. Local clusters for tetrahedral silicas have been shown to distinguish between all the crystalline polymorphs of silica and between crystalline and amorphous networks [12]. For example, Fig. 10a illustrates the local cluster for cristobalite, in which all tetrahedra are topologically identical and comprise *only* primitive 6-rings. A tetrahedron in a {4,2} tree network of vertex-sharing tetrahedra has 4 first-neighbor tetrahedra, 12 second neighbors, 36 third neighbors and 108 fourth neighbors, by which it can be seen from the neighbor counts in Fig. 10a that rings indeed serve to reduce the density of tetrahedra; larger rings are conversely able to increase configurational density because larger rings (> 6) are less rigid than smaller rings [5]. Because they are only displacive and not reconstructive modifications, the high- (β) and low-temperature (α) forms of each silica polymorph share the same polymorph topology and local cluster.

The α and β forms of Si_3N_4 and of SiC are, however, topologically distinct polymorphs. Fig. 10b depicts the

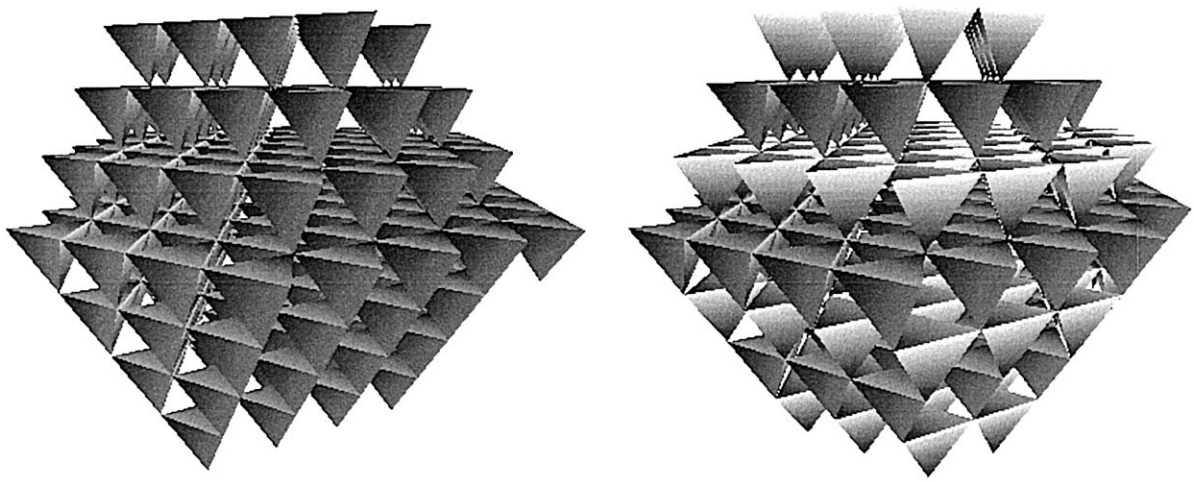

(a) (b)

Fig. 9. 200-tetrahedron models of (a) β-SiC, assembled according to the rules given in Fig. 7, and (b) α-SiC, assembled according to the rules given in Fig. 8a.

Table 2
Inter- and intra-tetrahedral angles and densities for rules-generated Si–X polymorphs

Polymorph	Node	Si–X–Si Angles θ (°)	Average Si–X–Si Angle θ (°)	Average X–Si–X Angle (°)	Model density ($\times 10^3$ kg/m^3)	Actual density ($\times 10^3$ kg/m^3)
β-Cristobalite	0	148	148	109.5	2.17	2.21
α-Cristobalite	0	145.3	145.3	109.5	2.33	2.33
Cristobalite-like a-SiO_2		Crystal basis: 148	146	109.4	2.29	2.20[a], 2.26[b]
β-Si_3N_4	0	109.5, 120, 125.1, 125.1	119.8	109.5	3.19	3.20
α-Si_3N_4	0	110.6, 114.2, 117.2, 118.1	118.3	109.5	3.22	3.20
		118.2, 118.4, 119.6,124.9				
	1	111.7, 113.1, 116.8, 120.3				
		120.6, 122.2, 123.0, 124.9				
	3	110.5, 115.6, 116.9, 117.3				
		117.8, 117.8, 117.8, 124.8				
	4	111.7, 113.1, 117.1, 117.7				
		117.9, 118.4, 119.6, 124.5				
a-Si_3N_4		Crystal basis: 119.8 (avg.)	119.6	109.5	3.42	–
β-SiC	0	109.5	109.5	109.5	3.21	3.21
α-SiC	0	109.5	109.5	109.5	3.24	3.22
a-SiC		Crystal basis: 109.5	112.0	109.6	3.25	2.86[c]

[a] Vitreous silica, annealed at 1273 K [30].
[b] Neutron-amorphized silica or quartz [30].
[c] Neutron-amorphized α-SiC [31].

local cluster of β-Si_3N_4, and Fig. 10c shows the two inequivalent local clusters for α-Si_3N_4. Like the local cluster of cristobalite, the local cluster of β-Si_3N_4 is compact and dominated by 6-rings, though with a substantial complement of 4-rings; the local clusters of α-Si_3N_4 exhibit a broader ring spectrum dominated by 5-rings. The even more compact local clusters of β- and α-SiC (Fig. 11) are identical in size and ring content, with equal numbers of 3- and 4-rings. Silicon carbide and silicon nitride polymorphs are denser than silica polymorphs (Table 2) because of the larger number of tetrahedra sharing a vertex.

4. Assembling amorphous networks

Local assembly rules require neither symmetry nor periodicity; the restrictions are those of underconnection and overlap of structuring polytopes. Because immediate local environments are generally supposed to differ little between crystalline and aperiodic forms, it is reasonable that assembly rules for non-crystalline forms can be based on slightly faulty versions of the assembly rules appropriate to crystalline polymorphs stable at the same conditions of temperature and pressure obtaining during formation of the amorphous phase [12]. Both initial *node offsets* and small changes in *rotation rules* may be used to generate structures lacking long-range order. Continued application of the modified rules results in structural defects that eventually alter local topology and impart topological disorder.

Additional algorithms are required to ensure maximal connectivity and to preclude intersection of tetrahedra. Connectivity was optimized by connecting shared vertices in adjacent nodes by Hookeian springs (with adjustable spring constants) that impose both forces and torques on the connecting vertices; the axial and rotational displacements of these springs were adjusted after each new tetrahedron was added so as to globally minimize the elastic energy stored in the springs [35]. Additional repulsive forces were applied to maintain steric exclusion and prevent intersection of tetrahedra. The global optimization procedure following each added tetrahedron connection was continued at least until the spring segment for that connection was less than half the Si–X distance; in some cases where large remanent spring segments remained, additional optimization was carried out until it was clear that little further reduction in spring length could be effected.

As a first example, the β-cristobalite rules modification given in Fig. 2b was chosen to specify 5° smaller rotation angles (85°) than occur in cristobalite. [2] Fig. 3b compares 200 nodes of a cristobalite-like amorphous silica (a-SiO_2) disordered structure, assembled according to these modified rules, to the ordered structure of β-cristobalite (Fig.

[2] Rules modifications using offset of the initial node, as used for amorphization of quartz [12], cannot be used for cristobalite, because node offsets around x or y affect only θ, as in the α–β transition, and around z have no effect because the rules rotations are defined about z.

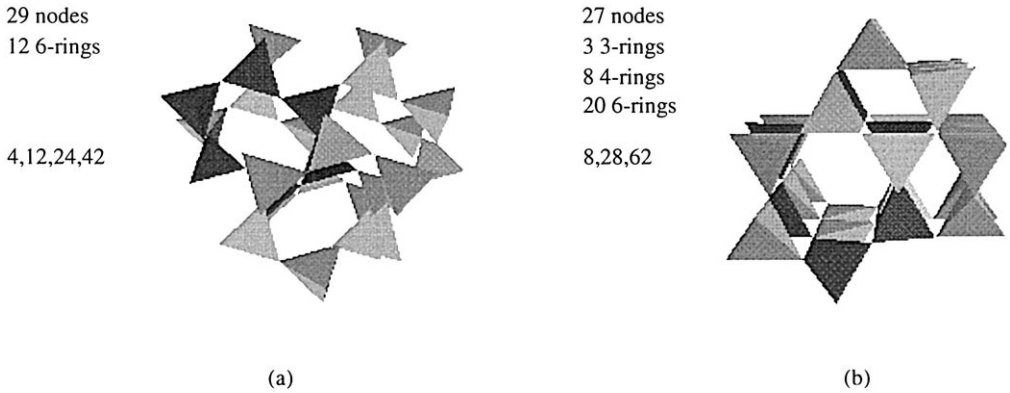

Fig. 10. Local clusters for (a) β-cristobalite SiO_2, (b) β-Si_3N_4, and (c) α-Si_3N_4, with cluster size, primitive ring distribution and number of first-, second-, third- (and fourth- for cristobalite) neighbor tetrahedra also indicated. α-Si_3N_4 has two inequivalent tetrahedron environments, hence two distinguishable local clusters. A 6-ring is highlighted in each cluster.

3a); the comparison reveals small but persistent differences in the tetrahedral arrangement that are reflected in a 5% densification (Table 2). While the tetrahedra remain relatively undistorted, as evidenced by the minimal remanent spring lengths (Fig. 3b) and the O–Si–O intra-tetrahedral angle distribution (Fig. 12), the Si–O–Si inter-tetrahedral angle distribution is significantly broad (Fig. 13), and the *average* Si–O–Si angle θ decreases slightly (Table 2).

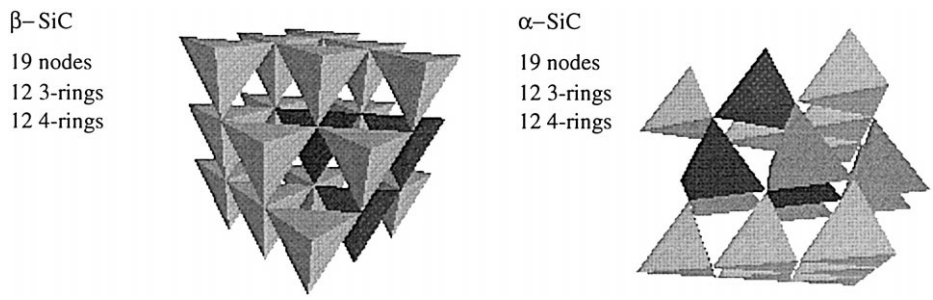

Fig. 11. Local clusters for (a) β-SiC and (b) α-SiC, with cluster size, primitive ring distribution and number of first-, second- and third-neighbor tetrahedra also indicated. A 3-ring is highlighted in each cluster.

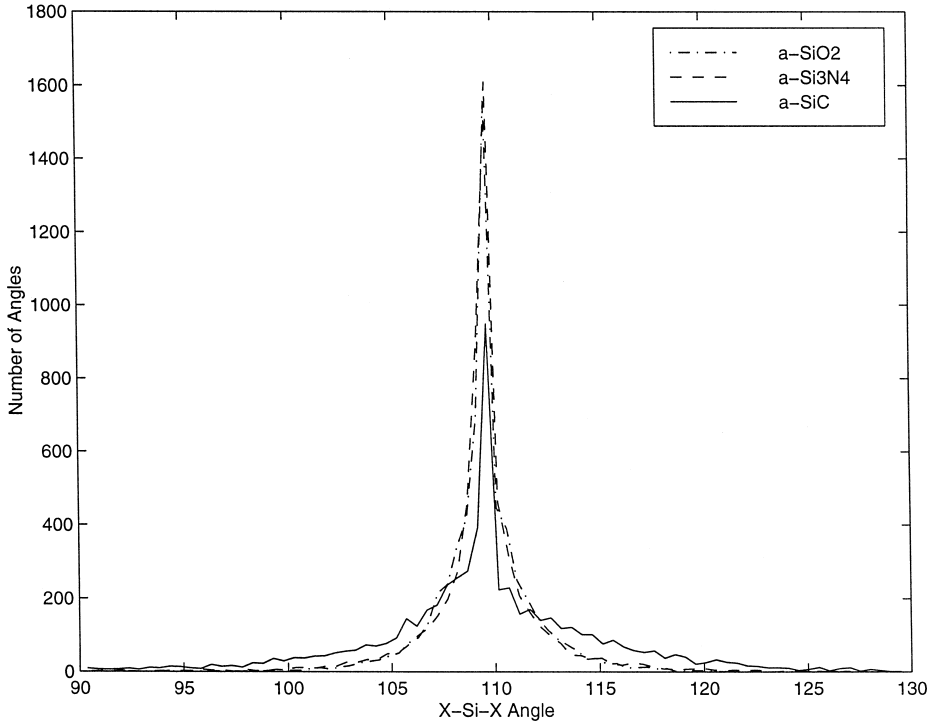

Fig. 12. Distribution of O–Si–O, N–Si–N, C–Si–C intra-tetrahedral angles for a-SiO_2, a-Si_3N_4 and a-SiC model assemblies.

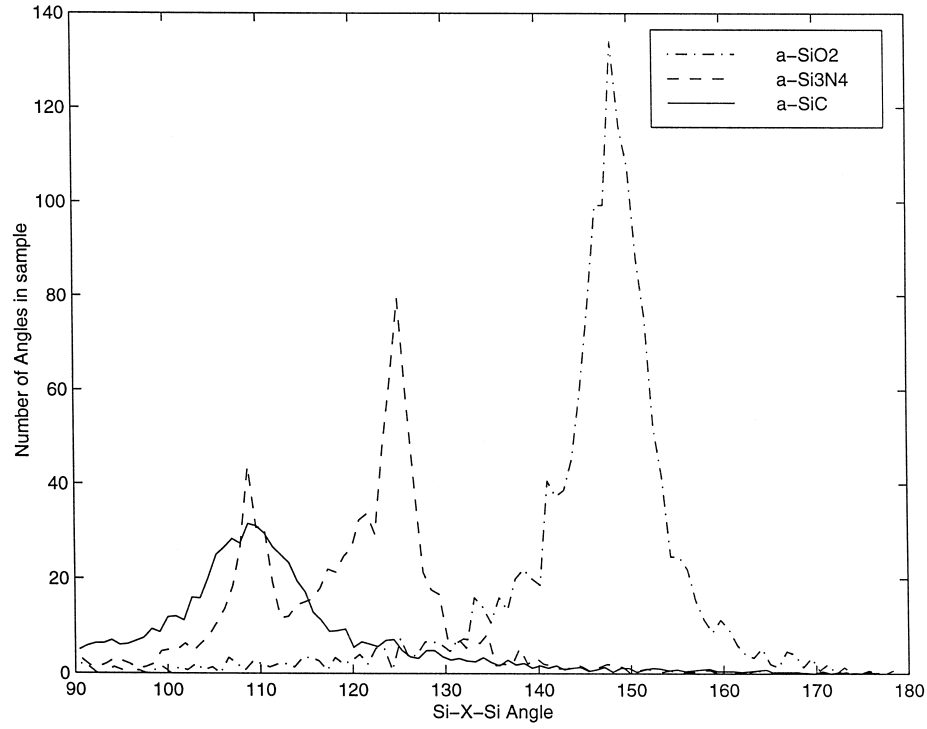

Fig. 13. Distribution of Si–O–Si, Si–N–Si, Si–C–Si inter-tetrahedral angle θ for a-SiO_2, a-Si_3N_4 and a-SiC model assemblies.

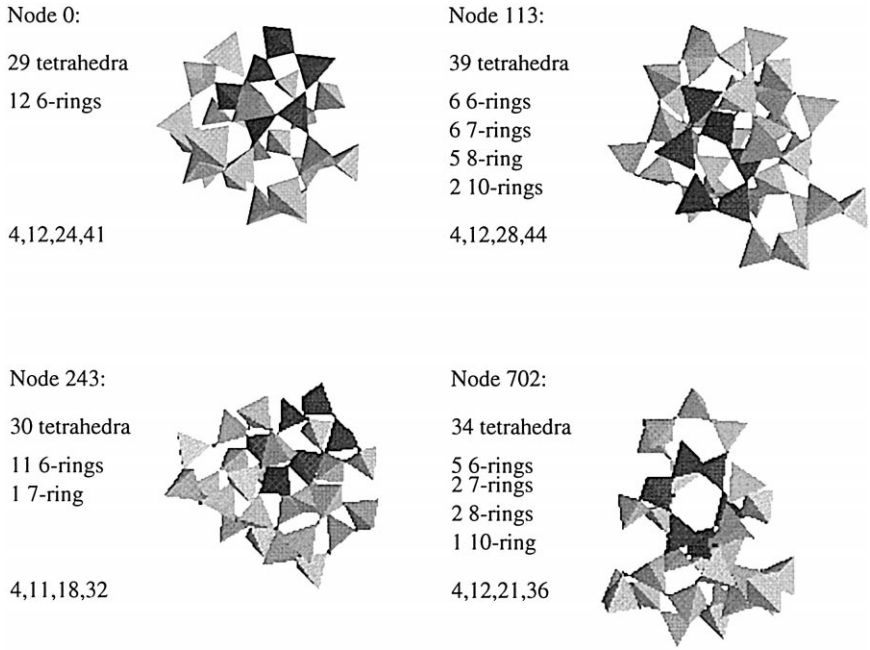

Fig. 14. Four local clusters from a cristobalite-like a-SiO_2 model assembled using the modified β-cristobalite rules given in Fig. 2b. The node designation begins with the initial tetrahedron (node 0), which retains a very cristobalite-like tetrahedron environment, and extends outward. Cluster size, primitive ring distribution and number of first- through fourth-neighbor tetrahedra are also indicated. A 6-ring is highlighted in each cluster.

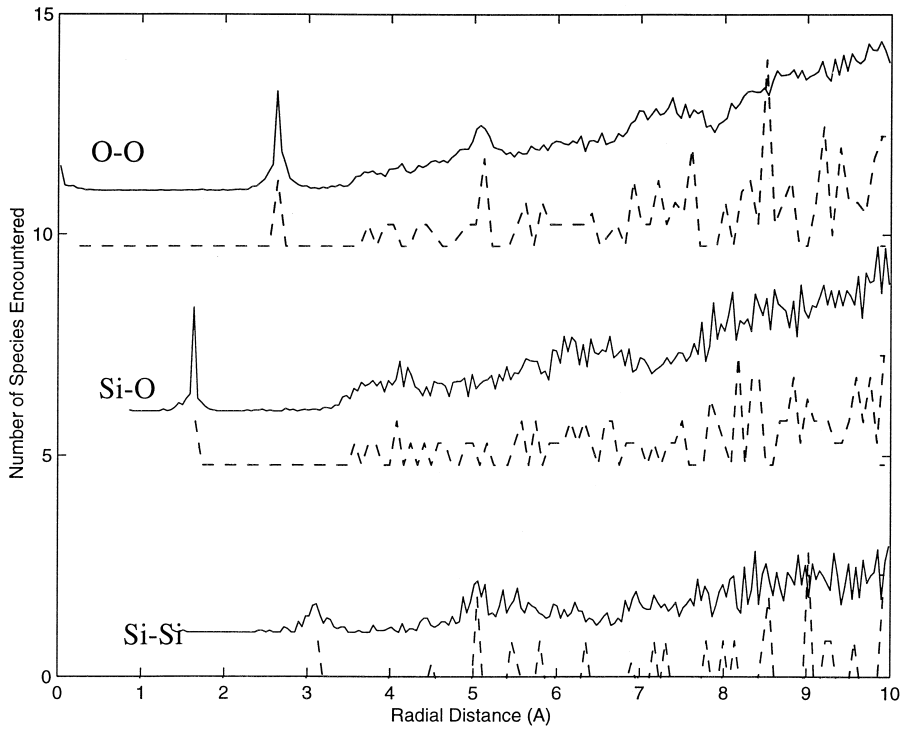

Fig. 15. Partial radial density functions (RDFs) for O–O (top), Si–O (middle) and Si–Si (bottom) correlations in cristobalite-like a-SiO_2 model (solid line) assembled using rules in Fig. 2b. The corresponding RDFs for β-cristobalite (dashed line) are superimposed for comparison, represented as triangular peaks rather than as delta functions.

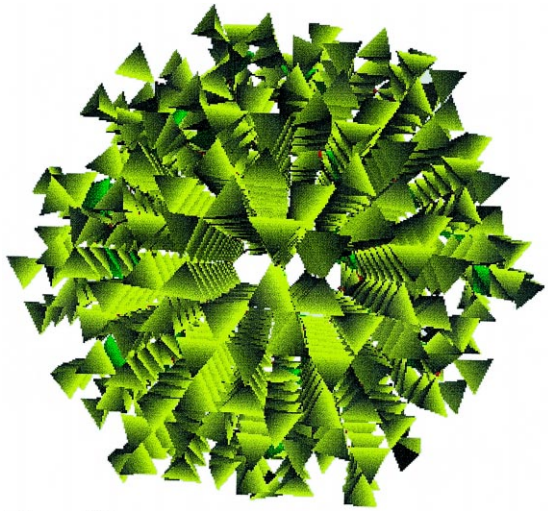

Fig. 16

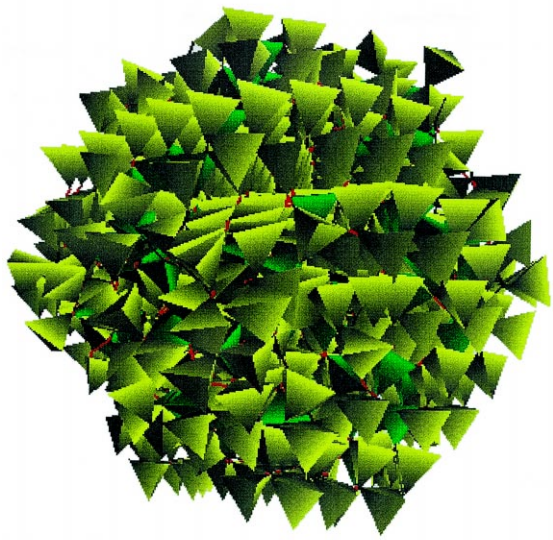

Fig. 17

Fig. 16. 1000 tetrahedra of a-Si_3N_4 assembled using modified rules in Fig. 5b. Green tetrahedra are underconnected, and red segments are remanent connection springs.

Fig. 17. 1000 tetrahedra of a-SiC assembled using modified rules in Fig. 8b. Underconnected tetrahedra and long remanent connection springs are much more in evidence than in Fig. 3b for a-SiO_2 or Fig. 16 for a-Si_3N_4.

Local clusters (Fig. 14) were extracted from the amorphous assemblage and document propagation of the disorder from the initial node (node 0), which retains a very cristobalite-like environment, extending outwards to node clusters of different size in which 6-rings no longer exclusively dominate. Radial density correlation functions (Fig. 15) were computed, using the method described earlier [12] involving averaging results from 50 tetrahedra randomly chosen from the centermost 10% of the silica assemblage. As well as reproducing the expected short-range Si–O and O–O tetrahedral correlations, these RDFs continue to retain some of the medium-range correlation features of the β-cristobalite crystal on which the modified rules were based, though less so for cristobalite-like a-SiO_2 than for amorphous silicas based on modification of quartz rules [12].

Modified rules used for assembling amorphous versions of Si_3N_4 and SiC are given in Fig. 5b and Fig. 8b, incorporating 5° rotation deviations from the rules for β-Si_3N_4 and α-SiC. An assemblage of 1000 tetrahedra of amorphous silicon nitride (a-Si_3N_4), assembled using the rules in Fig. 5b, is shown in Fig. 16. An analogous assemblage for a-SiC, assembled using the rules in Fig. 8b, is compared in Fig. 17. Significantly, 200 tetrahedra were insufficient in the a-Si_3N_4 model to reveal appreciable differences from β-Si_3N_4; even at 1000 tetrahedra, the disorder was slow to propagate, and the most striking feature of the assemblage is the underconnected tetrahedra (labelled green). Tetrahedral distortions are also present as another means of accommodating the rotation deficit, as evidenced by the breadth of the N–Si–N tetrahedral bond–angle distribution (Fig. 12), though the average angle (Table 2) remains centered on the 109.5° tetrahedral ideal. The extracted local clusters show (Fig. 18) that local topological disorder has in fact propagated, though 6-rings still generally dominate and the computed radial density functions (Fig. 19) remain extremely crystal-like. The three families of Si–N–Si angles found in crystalline β-Si_3N_4 persist in the topologically disordered assembly (Fig. 13), though broadened and shifted to slightly larger angles (in contrast to silica where the average Si–O–Si angle was found to decrease).

The 1000 tetrahedron a-SiC assembly shown in Fig. 17 exhibits more evidence of topological disorder, but only at a cost of extensive underconnection and substantial tetrahedral distortion. The distortion is evidenced by long inter-vertex springs in the assemblage and a broad C–Si–C (Fig. 12) angle distribution, or equivalently by the broad Si-C–Si angle distribution (Fig. 13), since in this {4,4} structure the Si–C–Si inter-tetrahedral angle is also the C–Si–C intra-tetrahedral angle. Because we have elected to define [SiC_4] units as the tetrahedra, instead of [CSi_4], the average C–Si–C angle remained close to tetrahedral, but the *average* Si–C–Si angle θ, which should be equivalently tetrahedral, has shifted by 2.5° to 112°, corresponding to a large distortion of [CSi_4] tetrahedra. Although the radial correlation density functions (Fig. 20) persist in crystal-like intermediate-range correlations, the local clusters (Fig. 21) differ markedly from those of β-SiC, largely in the dominant appearance of 5-rings from the opening up of 3- and 4-rings as a consequence of the pervasive underconnection.

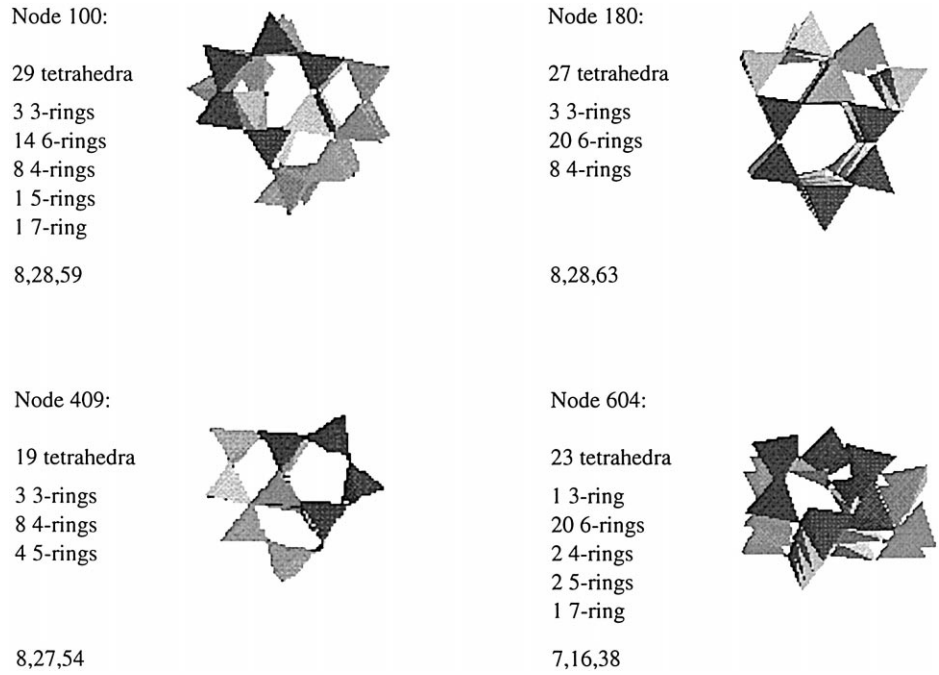

Fig. 18. Four local clusters for the a-Si_3N_4 assembly in Fig. 16. A 5-ring is highlighted in the cluster for node 409, a (dominant) 6-ring in each of the other clusters.

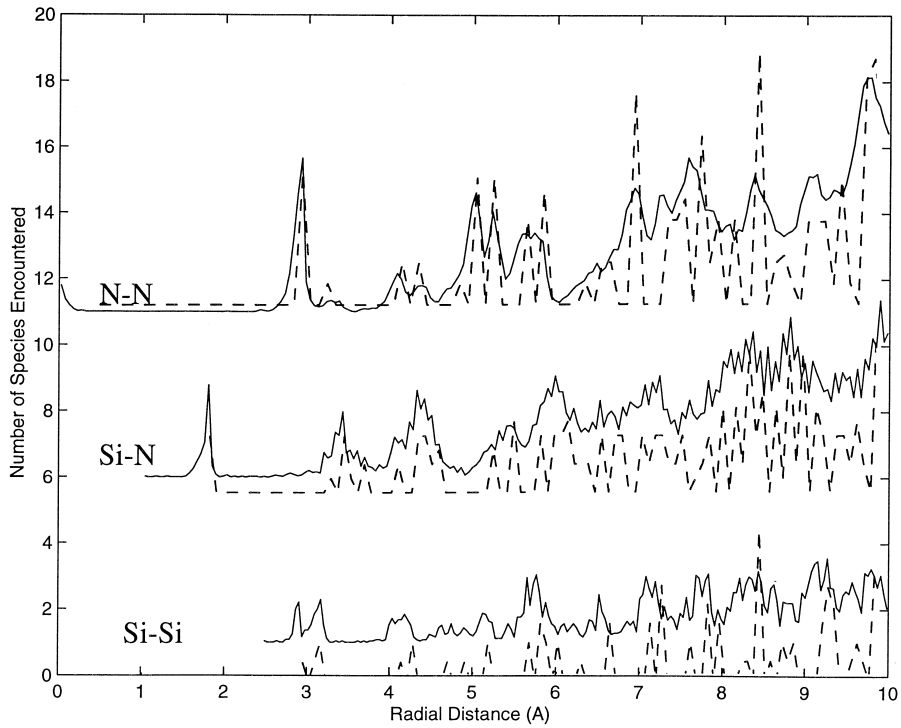

Fig. 19. Partial radial density functions for N–N (top), Si–N (middle) and Si–Si (bottom) correlations in the a-Si_3N_4 model (solid line) in Fig. 16. RDFs for β-Si_3N_4 (dashed line) are superimposed.

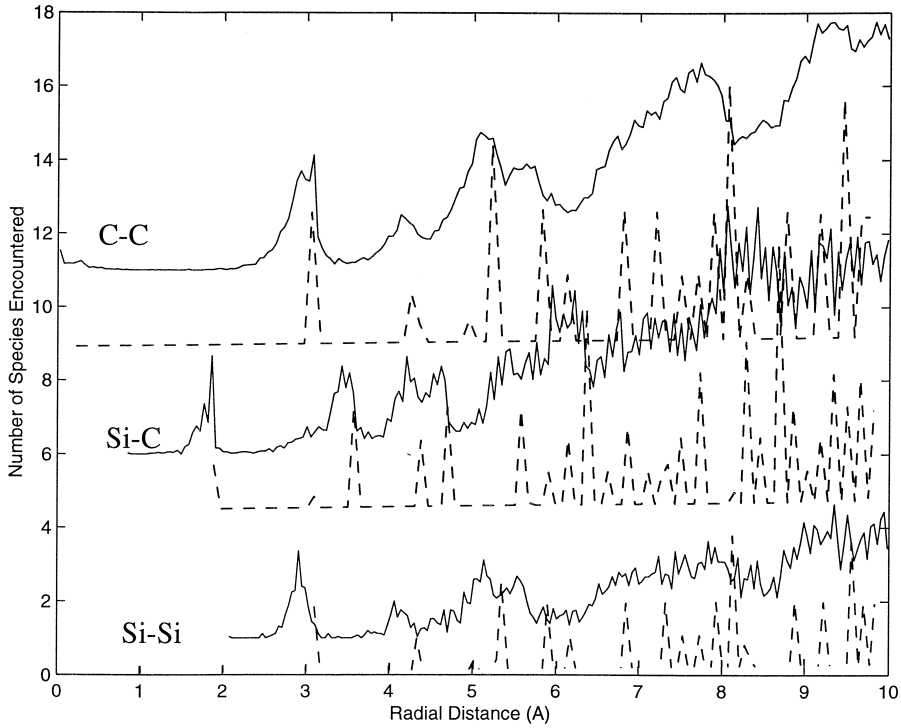

Fig. 20. Partial radial density functions for C–C (top), Si–C (middle) and Si–Si (bottom) correlations in the a-SiC model (solid line) in Fig. 17. RDFs for α-SiC (dashed line) are superimposed.

The degree of underconnection in all models was quantified by counting unbonded tetrahedron vertices and tabulating the percentage of underbound tetrahedra by the number of missing connections (Table 3). The quantitative result confirms the qualitative impression from inspection that the a-SiC model is substantially less connected than

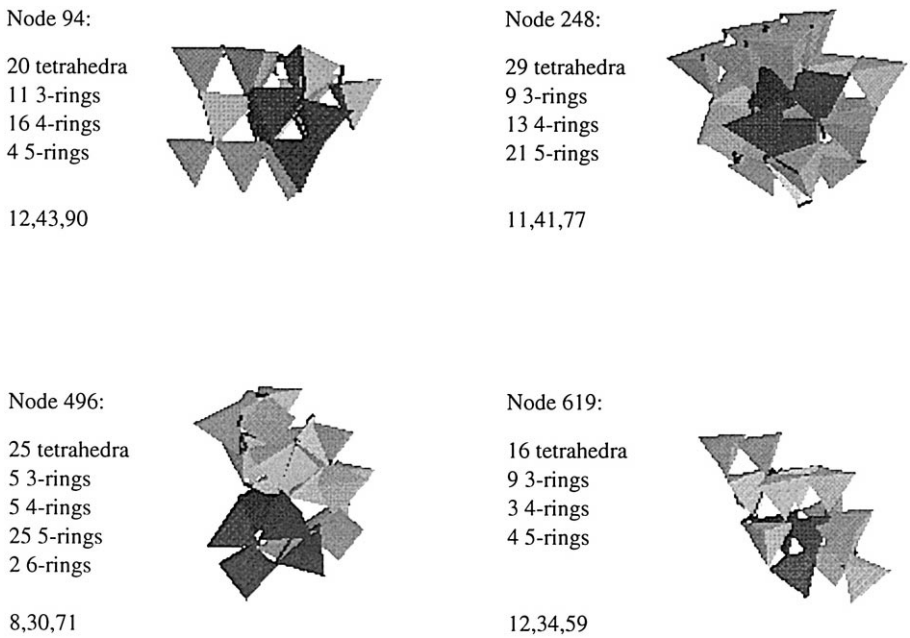

Fig. 21. Four local clusters for the a-SiC assembly in Fig. 17. A 4-ring is highlighted in each cluster. Black rods are remanent connection springs.

Table 3
Percent underconnected tetrahedra in model amorphous networks as a function of number of absent nearest neighbor tetrahedra

Network model	0	1	2	3	4	5	6	7	8	9	10	11	Σ
a-SiO_2	62.4	9.8	8.7	19.1									37.6
a-Si_3N_4	60.3	5.5	1.1	0.2	0.9	8.7	14.7	2.9					39.7
a-SiC	49.7	11.7	4.0	1.2	0.6	0.1	0.8	1.6	6.2	8.4	9.6	6.1	50.3

are a-SiO_2 and a-Si_3N_4 models. A sizeable (and unquantifiable with the present counting algorithms) fraction of these underconnected tetrahedra are underbound because they reside at the surface. A rough estimate of the surface contribution can be made by enumerating all tetrahedra bound to the structure through only two vertices (those tetrahedra in SiO_2 missing two connections, in Si_3N_4 missing four, in SiC missing six), which are most likely to be surface tetrahedra; removing these from the total number of tetrahedra in the model leaves the interior tetrahedra, on which basis the underbound percentages can be recalculated. By this estimate, the a-SiO_2 is 86.4% connected, a-Si_3N_4 89.9% connected, but a-SiC only 73.8% connected. Better estimates await an improved counting algorithm that specifically enumerates surface tetrahedra, but the substantial underconnection of a-SiC is nonetheless qualitatively apparent in the assembly depiction.

All three amorphized models were found to densify to varying extents. Experimentally, the density for vitreous silica [30] is about the same as the least dense form of cristobalite, but both densify to the radiation-induced metamict silica state [30]. Both silicon carbide polymorphs dilate by 10–11% when amorphized by neutrons [31], which swelling could be dominated by point defect (e.g., C vacancies, Si interstitials and C_{Si} anti-site defects), rather than network changes. The densification in the present amorphous models is at least in part (and counter-intuitively) due to the underconnection, which arises because insufficient inter-tetrahedron repulsion forces were included. If the tetrahedra were forced to stay farther apart (a structural principle known as *eutaxy* [36]) and thus lower the density, connectivity could actually be improved.

5. Topological implications for amorphizability

The assembly procedures outlined for generating amorphous structures from SiO_2, Si_3N_4 and SiC provide some insights into the respective amorphizabilities of the three compounds. Substantial topological disorder is relatively easy to propagate in {4,2}-connected silica, for even modest deviations from crystalline assembly rules. The resulting amorphous assemblages were substantially connected and exhibited little tetrahedral distortion. A similar finding is made for topologically modeled reconstructions of collision cascades in SiO_2 which we report elsewhere [13,37]. The explanation can be seen in the considerable multiplicity of options afforded in these marginally connected networks, in particular the independence of the inter-tetrahedral Si–O–Si angles from each other, and from the O–Si–O intra-tetrahedral angles.

It appears possible to propagate topological disorder also in Si_3N_4 assemblies with the same extent of rules deviation, the resulting arrangements suffering from about the same underconnection and tetrahedral distortion as for silica, in agreement with molecular dynamics simulations [7,8]. But the overall amorphized Si_3N_4 structure is seen to remain much more crystal-like than silica, doggedly retaining many of the same intermediate and long-range correlations exhibited by its crystalline analogue. The local clusters, while topologically distinct and incorporating some new elements, do not stray far from the local cluster of the crystalline arrangement. The difficulty in amorphizing Si_3N_4 by irradiation may lie in this reluctance to cede intermediate- or long-range order, or in related problems associated with acceptable reconnection following cascade randomization, as explored in a companion paper [13].

By contrast, topological disorder in SiC proved difficult to propagate acceptably, even in assembly models with only modest rules deviations applied. As with Si_3N_4, though the local topology developed a new element (dominant 5-rings in this case), the propagation attempt retained most of the intermediate-range correlations of the crystalline form on which the rules are based. Assembly was accomplished only at an accompanying (and probably energetically unacceptable) cost of substantial underconnection and large tetrahedral distortion. It is clear that one reason is strong interdependence of the four Si–C–Si angles at a given vertex and the interrelation of the Si–C–Si and C–Si–C tetrahedral angles for the {4,4} connectivity. As indicated earlier (Section 2), both α and β forms of SiC nevertheless amorphize under irradiation almost as readily as do crystalline silicas, with an ease very much at variance with the predictions of topological freedom and also with the results of the present modeling study, both of which imply great difficulty in propagating topological disorder in chemically ordered SiC.

The admission of chemical *disorder* as a possibility substantially alters the topological basis assumed for the modeling, as noted earlier. Only if [SiC_4] (or equivalently [CSi_4]) chemical units do not keep intact during irradiation (or other amorphizing treatment) are the rigidity constraints relaxed sufficiently for amorphization to occur. Indeed, evidence both from experiment [14,18–23,26] and

from molecular dynamics simulations [38] supports the view that topological disorder in SiC arises from point-defect accumulation rather than from in-cascade amorphization. The imposition of chemical disorder thus represents a pre-condition (or at least a co-condition) for amorphization, and the resulting metamict SiC is likely to exhibit a high density of anti-site configurations. Unlike silica (and perhaps Si_3N_4), the integrity of the chemical coordination polytope cannot be preserved upon amorphization if {4,4} connectivity is to be maintained.

6. Conclusions

Local rules-based assembly has been shown to represent a viable method by which to investigate the topology of crystalline Si-based tetrahedral network compounds and the topological constraints associated with the propagation of topological disorder required for amorphization of their tetrahedral networks. The assembly rules proved surprisingly simple, even for crystallographically complex α-Si_3N_4 and the highly over-connected SiC networks, and provide an easily implemented method for rapidly erecting large crystalline models for subsequent manipulation. The local clusters (and their associated ring complement) provide a useful and essentially complete assessment of local topology and a characteristic structural unit in which differences are readily recognized. In common with several silica polymorphs already investigated [12], α-Si_3N_4 was found to have two topologically inequivalent local clusters.

Topological disorder was found relatively easy to propagate in SiO_2 and Si_3N_4 during assembly. SiC could not be disordered in assembly without significant underconnection and tetrahedral distortion, which could both prove energetically unacceptable. The modeling procedure provided easy access to the relevant structural parameters of bond angles, density, topology and radial correlations. The methodology demonstrates the extent to which topology alone may dictate structural options and can provide useful insights when applied to analysis of results from full-blown molecular dynamics modeling of network structures.

Acknowledgements

This work was funded by the Office of Basic Energy Science, US Department of Energy through grant DE-FG02-89ER45396, to whom two of us (L.W.H., C.E.J.) are much indebted for support. The authors acknowledge very helpful discussions with Dr Steven J. Zinkle of Oak Ridge National Laboratory and Dr Kurt A. Sickafus of Los Alamos National Laboratory and also the referees' constructive comments. The authors are likewise grateful to Professor Bonnie Berger of the Department of Mathematics and the Laboratory for Computer Science (LCS) at MIT for substantive discussions about local rules-based assembly procedures, for provision of computational facilities through the assistance of the Advanced Research Projects Agency under contract N0014-95-1-1246 which funds the Computational Biology Group in LCS, and for providing one of us (VP) with an research assistantship supported by Department of Energy grant DE-FG02-95ER25253.

References

[1] S. Dutton, D.J.R. Taylor, R.F.T. Stepto, Die Angewandte Makromol. Chemie 240 (1996) 39.
[2] B.A. Berger, P.W. Shor, L. Tucker-Kellogg, J. King, Proc. Natl. Acad. Sci. USA 91 (1994) 7732.
[3] P.K. Gupta, J. Non-Cryst. Solids 195 (1996) 158.
[4] P.K. Gupta, A.R. Cooper, J. Non-Cryst. Solids 123 (1990) 14.
[5] L.W. Hobbs, J. Non-Cryst. Solids 182 (1995) 27.
[6] S.J. Zinkle, Nucl. Instr. and Meth. B 91 (1994) 234.
[7] P. Vashishta, A. Nakano, R.K. Kalia, I. Ebbsjö, J. Non-Cryst. Solids 182 (1995) 59.
[8] P. Vahishta, R.K. Kalia, A. Nakano, W. Li, I. Ebbsjö, in: M.F. Thorpe, M.I. Mitkova (Eds.), Amorphous Insulators and Semiconductors, Kluwer Academic, Dordrecht, 1997, p. 151.
[9] P.K. Gupta, J. Am. Ceram. Soc. 76 (1993) 1088.
[10] L.W. Hobbs, Nucl. Instr. and Meth. B 91 (1994) 30.
[11] L.W. Hobbs, A.R. Sreeram, C.E. Jesurum, B.A. Berger, Nucl. Instrum. and Meth. B 116 (1996) 18.
[12] L.W. Hobbs, C.E. Jesurum, V. Pulim, B. Berger, Local topology of silica networks, Philos. Mag. A 78 (1998) in press.
[13] L.W. Hobbs, C.E. Jesurum, V. Pulim, Topological modeling of cascade amorphization in network structures using local rules, Mater. Sci. Eng. A (1998) in press.
[14] W.J. Weber, L.M. Wang, Nucl. Instr. and Meth. B 4 (1995) 298.
[15] J.K.N. Lindner, R. Zuschschlag, E.M. Te Kaat, Nucl. Instr. and Meth. B 62 (1992) 314.
[16] R.K. Eby, R.C. Ewing, R.C. Birtcher, J. Mater. Res. 7 (1992) 3080.
[17] W. Bolse, S.D. Peteves, F.W. Saris, Appl. Phys. A 58 (1994) 493.
[18] H. Inui, H. Mori, H. Fujita, Philos. Mag. B 61 (1990) 107.
[19] A. Matsunaga, C. Kinoshita, K. Nakai, Y. Tomokiyo, J. Nucl. Mater. 179–181 (1991) 457.
[20] H. Inui, H. Mori, T. Sakata, Philos. Mag. B 65 (1992) 1.
[21] H. Inui, H. Mori, T. Sakata, Philos. Mag. B 66 (1992) 737.
[22] W.J. Weber, L.M. Wang, N. Yu, Nucl. Instr. and Meth. B 116 (1996) 322.
[23] S.J. Zinkle, L.L. Snead, Nucl. Instrum. and Meth. B 116 (1996) 92.
[24] E. Wendler, A. Heft, W. Wesch, Ion-beam induced damage and annealing behaviour in SiC, Nucl. Instrum. and Meth. B 141 (1998) in press.
[25] W. Bolse, Formation and development of disordered networks in Si-based ceramics under ion bombardment, Nucl. Instr. and Meth. B 141 (1998) in press.

[26] L.L. Snead, S.J. Zinkle, Mater. Res. Soc. Symp. Proc. 439 (1997) 595.
[27] A.F. Wells, Structural Inorganic Chemistry, 3rd edn. Clarendon Press, Oxford, 1967, p. 236.
[28] G.D. Watkins, in: J.H. Crawford Jr., L.M. Slifkin (Eds.), Point Defects in Solids, Vol. 2, Semiconductors and Molecular Crystals, Plenum, London, 1972, p. 333.
[29] A.G. Revesz, G.V. Gibbs, in: G. Lucovsky, S.T. Pantelides, F.L. Galeener (Eds.), The Physics of MOS Insulators, Pergamon, New York, 1980, p. 92.
[30] W. Primak, Phys. Rev. 110 (1958) 1240.
[31] L.L. Snead, S.J. Zinkle, J.C. Hay, M.C. Osborne, Amorphization of SiC under ion and neutron irradiation, Nucl. Instr. and Meth. B 141 (1998) in press.
[32] J.F. Shackelford, J. Non-Cryst. Solids 204 (1996) 205.
[33] C.S. Marians, L.W. Hobbs, J. Non-Cryst. Solids 106 (1988) 317.
[34] K. Goetzke, H.-J. Klein, J. Non-Cryst. Solids 127 (1991) 215.
[35] C.E. Jesurum, V. Pulim, B. Berger, L.W. Hobbs, Mater. Res. Soc. Symp. Proc. 439 (1997) 633.
[36] M. O'Keeffe, Acta Crystallogr. A 33 (1977) 924.
[37] L.W. Hobbs, C.E. Jesurum, V. Pulim, Modeling the cascade amorphization of silicas with local-rules reconstruction, Nucl. Instr. and Meth. B 141 (1998) in press.
[38] T. Diaz de la Rubia, M.-J. Caturla, M. Tobin, Mater. Res. Soc. Symp. Proc. 373 (1995) 555.